Vol. 22, No. 3(2023) IA2367
Revista Mexicana de Ingeniería Química

Biosynthesis of gold nanoparticles using the aqueous extract of *Hippocratea excelsa* root bark. Antioxidant and photocatalytic evaluation

Biosíntesis de nanopartículas de oro utilizando el extracto acuoso de la corteza de raíz *Hippocratea excelsa*. Evaluación antioxidante y fotocatalítica

C. Nuñez-Delgado[1], A. Luna-Flores[1], L.A. Conde-Hernández[1], E. Flores-Aquino[2], A. Romero-López[3], N. Tepale[1]*

[1]*Facultad de Ingeniería Química, Benemérita Universidad Autónoma de Puebla, Puebla, CP 72570, México.*
[2]*Departamento de Nanocatálisis, Centro de Nanociencias y Nanotecnología, Universidad Nacional Autónoma de México, Ensenada, Baja California, CP 22860, México.*
[3]*Instituto de Física, Benemérita Universidad Autónoma de Puebla, Puebla, CP 72570, México.*

Received: June 20, 2023; Accepted: August 28, 2023

Abstract

In this study the biosynthesis of gold nanoparticles (AuNPs) using the aqueous extract of the root bark of *Hippocratea excelsa* (HE) is reported. AuNPs were synthesized by adding different volumes of HE extract, ranging from 0.2-1 mL, and utilizing the gold precursor at 0.25 and 1 mM. All reactions were synthesized at room temperature. The AuNPs were characterized by UV-vis, TEM, DLS, Z-potential, and XRD. Extract and AuNPs antioxidant capacity was obtained by ABTS and DPPH methods. The photocatalytic activity was tested with methylene blue (MB) dye degradation. The UV-vis spectra showed a band associated with the gold surface plasmon resonance (SPR) at around 535 nm, evidencing the presence of nanoparticles. The hydrodynamic diameter suggests that the biomolecules of the extract attach to the nanoparticles, while the Z-potential reveals a stable colloidal solution. Micrographs demonstrated predominantly spherical AuNPs with a size of approximately 25 nm. XRD analysis confirmed the face cubic center (fcc) structure of the nanoparticles. On the other hand, the extract exhibited better antioxidant properties than the AuNPs. Finally, the photocatalytic experiments reveal an MB dye degradation of up to 89%. These results show that AuNPs produced by ecological and simple methods could be used in different applications.

Keywords: biosynthesis, nanoparticles, *Hippocratea excelsa*, antioxidant, photocatalysis.

Resumen

En este estudio se reporta la biosíntesis de nanopartículas de oro (AuNPs) utilizando el extracto acuoso de la corteza de raíz *Hippocratea excelsa* (HE). Las AuNPs se sintetizaron agregando diferentes volúmenes del extracto, desde 0.2 hasta 1 mL. Además, se utilizó el precursor de oro a 0.25 y 1 mM. Todas las reacciones se sintetizaron a temperatura ambiente. Las AuNPs se caracterizaron mediante espectroscopía UV-vis, TEM, DLS, Potencial Z, y XRD. La capacidad antioxidante del extracto y de las AuNPs se obtuvo con los métodos ABTS y DPPH. La actividad fotocatalítica se probó con la degradación del colorante azul de metileno (MB). Los espectros UV-vis mostraron una banda asociada a la resonancia del plasmón superficial (SPR) del oro alrededor de 535 nm, evidenciando la presencia de nanopartículas. El diámetro hidrodinámico sugiere que las biomoléculas del extracto se adhieren a las nanopartículas, mientras que el potencial Z evidencia una solución coloidal estable. Las micrografías mostraron AuNPs predominantemente esféricas con un tamaño aproximado de 25 nm. Los análisis XRD confirmaron la estructura fcc de las nanopartículas. Por otra parte, el extracto mostró mejores propiedades antioxidantes que las AuNPs. Finalmente, los experimentos de fotocatálisis revelan una degradación del colorante MB hasta del 89 %. Estos resultados muestran que las AuNPs producidas por métodos simples y ecológicos podrían ser utilizadas en diferentes aplicaciones.

Palabras clave: biosíntesis, nanopartícula, *Hippocratea excelsa*, antioxidante, fotocatálisis.

*Corresponding author. *E-mail*: nancy.tepale@correo.buap.mx;
https://doi.org/10.24275/rmiq/IA2367
ISSN:1665-2738, *issn-e*: 2395-8472

1 Introduction

In recent years, great interest in green chemistry has emerged as a viable option for synthesizing nanoparticles. This is because traditional physical and chemical methods can be toxic to the environment and often require too much energy (Serrano-Niño *et al*., 2020; Ying *et al*., 2020). Green synthesis or biosynthesis from plant extracts is being implemented in the production of nanoparticles (NPs) due to its simplicity and sustainability (El-Borady *et al*., 2020; Kumari & Meena, 2020). Biosynthesis presents advantages, such as low cost, short production times, industrial scalability, and biocompatibility (Doan *et al*., 2020; Kamran *et al*., 2019; Keijok *et al*., 2019; Kumari & Meena, 2020). Gold, synthesized at the nanometric level, is widely studied due to its ability to interact with light thanks to its Surface Plasmon Resonance (SPR) (Kurhade *et al*., 2021), its resistance to oxidation, its long-term stability, and its biocompatibility (Kumari & Meena, 2020). Therefore, AuNPs are applied in various areas, such as chemical engineering, catalysis, medicine, optics, and electronics (Cordero-García *et al*., 2023; Irfan *et al*., 2016; Kurhade *et al*., 2021). Some plants have been used to produce AuNPs, such as *Eryngium heterophyllum*, *Amphipterygium adstringens* (Aguilar-Pliego *et al*., 2021), *Hypericum perforatum* (Serrano-Niño *et al*., 2020), *Nigella arvensis* (Chahardoli *et al*., 2018), *Camellia sinensis* (T. Singh *et al*., 2020), and *Petroselinum crispum* (El-Borady *et al*., 2020). The plant extract and the reaction conditions play a fundamental role in the shape and size of the NPs (Aji *et al*., 2022; Kamran *et al*., 2019). Leaves, stems, roots, flowers, and seed extracts contain various phytochemicals (flavonoids, aldehydes, ketones, amines, carboxylic acids, phenols, terpenes, sugars, proteins, and alkaloids) that render their use feasible as reducing and stabilizing agents in the synthesis of NPs (Irfan *et al*., 2016; Kurhade *et al*., 2021; J. Singh *et al*., 2018; T. Singh *et al*., 2020). In addition to their reduction capacity, some plants have medicinal value, highlighting their antioxidant, anti-inflammatory, antibacterial, antifungal, and anticancer properties (Chahardoli *et al*., 2018; Kurhade *et al*., 2021).

In Mexico, the use of medicinal plants is a common practice. Therefore, its study comprises an area of great opportunity. It is desirable to study and understand the role of bioactive agents and even to take advantage of their medicinal properties. With such knowledge, it is possible to design new materials that can be used for potential applications. Aguilar Pliego *et al*., (2021) synthesized gold clusters and AuNPs using extracts of toad leaf (*Eryngium heterophyllum*) and cuachalalate (*Amphipterygium adstringens*), two plants with medicinal uses in Mexico. The materials were immobilized on a support, and their catalytic activity was tested.

The bark of the stems and roots of the *Hippocratea excelsa* (HE) plant, commonly known in the central part of Mexico as "cancerina" has been used to treat various diseases (gastric ulcers, kidney diseases, skin conditions, uterine infections, as an anti-inflammatory, as a healing agent, and for the treatment of dysentery) (Alanís *et al*., 2005; Apaza Ticona *et al*., 2022; Escobedo Hinojosa *et al*., 2014; Mena-Rejón *et al*., 2007; Navarrete *et al*., 2002; Velázquez *et al*., 2006). This plant contains active compounds such as tingenone, celastrol, galactitol, pristimerin, excelsine, friedelin, canophyllol, canophyllal, canophyllic acid, triterpenes, sesquiterpene evoninoate and pyridine alkaloids (Cáceres-Castillo *et al*., 2008; Calzada & Mata, 1995; Furukawa *et al*., 2002, 2018; Mata *et al*., 1990; Mena-Rejón *et al*., 2007; Navarrete *et al*., 2002; Perez *et al*., 1995; Reyes-Chilpa *et al*., 2003). These molecules make this plant a potent reducing agent in the synthesis of NPs. As far as we know, there hasn't been any report on the synthesis of AuNPs using the HE extract. In addition, the synthesis does not require any external surfactant, reducing, or capping agent. Therefore, based on scientific studies of the plant, we hypothesized that HE extract is rich in esters, hydroxyl, and ketone groups, which make it an excellent candidate for this process.

The biosynthesis of AuNPs using the aqueous extract of the *Hippocratea excelsa* root bark was investigated. The characterization of the synthesized AuNPs was carried out through various techniques such as UV-vis spectroscopy, Dynamic Light Scattering (DLS), Transmission Electron Microscopy (TEM), and X-ray Diffraction (XRD). Furthermore, the antioxidant activity of both the extract and the AuNPs using ABTS and DPPH assays was evaluated. Finally, the photocatalytic activity of the synthesized AuNPs in the degradation of the MB model molecule was tested.

2 Materials and methods

2.1 Reagents

$HAuCl_4 \cdot 3H_2O$ (Sigma-Aldrich) and tri-distilled water (Hycel de México S.A. de C.V.) were used, without further purification. The root bark of *Hippocratea excelsa* (HE) was purchased from a medicinal plant shop in Puebla, Mexico.

2.2 Preparation of the HE extract

The root bark of HE was washed with tri-distilled water. It was finely cut and shade-dried at room

temperature for 5 days. Ten g of the root bark was placed in 100 mL of tri-distilled water and added to a flask with constant stirring. The mixture was boiled for 10 min on a heating plate. The cooled solution was centrifuged for 5 min at 5,800 rpm to remove solid matter, and it was filtered through Whatman paper and stored at 4°C.

2.3 Biosynthesis of AuNPs

AuNPs synthesis was carried out using different volumes of HE aqueous extract, ranging from 0.2 mL to 1 mL, both pure and diluted in water at a 1:1 ratio. In addition, it was used 10 mL of $HAuCl_4 \cdot 3H_2O$ aqueous solution with concentrations of 0.25 and 1 mM. All reactions were performed at room temperature. To measure the antioxidant and photocatalytic properties, the samples were used (1) directly and (2) washed with distilled water a couple of times (centrifuged at 15,000 rpm for 15 min).

2.4 Characterization

The optical properties of the colloidal gold solutions were studied and analyzed by UV-visible spectroscopy utilizing a GENESYS 10S spectrophotometer (Thermo Scientific) at 25°C and quartz cells with an optical path of 1 cm. The hydrodynamic diameter was measured from the colloidal gold solutions with a Dynamic Light Scattering System (DLS; Malvern Zetasizer Nano ZS, Malvern Instruments Worcestershire, UK) equipped with a He-Ne laser (λ = 633 nm) with 4.0 mW power and backscattering mode. The Z-potential measurements were carried out with the Zeta-Sizer IV system (Malvern Instruments Worcestershire, UK) under the same conditions as the ones used with the DLS system. The size and shape of the AuNPs were determined by TEM analysis utilizing a JEOL-JEM-2010 in conventional transmission mode, operating at 80 kV. For this characterization, samples were prepared by placing a drop of the solution onto a carbon-coated Cu grid. X-ray diffraction (XRD) patterns were measured using an X-ray diffractometer from Panalytical (model Empyrean, Almelo, Netherlands) with Cu Kα radiation (λ = 1.5406 Å) and a Ni filter. The acceleration voltage and the applied currents were 40 kV and 35 mA, respectively. Data were collected with a step width of 0.17° (2θ) from 10° to 90° (2θ).

2.5 Antioxidant properties assay

Eighty microliters of the plant extract (10, 20, 30, 40, and 50 μL/mL) or AuNPs samples were added to 3,920 mL of the ABTS.+ radical-ethanol solution. The solutions were perfectly homogenized (initial absorbance) and were allowed to stand for 7 min (final absorbance). Absorbance was measured at 517 nm with a UV-vis spectrophotometer (Conde-Hernández & Guerrero-Beltrán, 2014). The percentage of inhibition was calculated by the following formula:

$$\% \text{ Inhibition ABTS} = \frac{\text{Initial Absorbance - Final Absorbance}}{\text{Initial Absorbance}} \times 100 \quad (1)$$

The DPPH free radical scavenging activity of the HE extract and AuNPs samples were tested by the standard method. Briefly, 3,900 μL of DPPH solution (0.06 mM in methanol) was mixed with 100 μL of different concentrations of HE extract (10, 20, 30, 40, and 50 μL/mL) or AuNPs samples. The reaction mixture was stirred well and incubated in the dark for 30 min. After incubation, absorbance was recorded at 517 nm against a blank. The scavenging percentage of the free radicals was determined by the following formula (Chahardoli *et al*., 2018):

$$\% \text{ Inhibition DPPH} = \frac{\text{Control Absorbance - Sample Absorbance}}{\text{Control Absorbance}} \times 100 \quad (2)$$

2.6 Degradation of MB

In brief, 5 mL of AuNPs colloidal solution was added to 40 mL of MB solution with a concentration of 5 ppm. The samples were placed under the direct action of the sun with constant agitation for 90 min. The degradation of the dye was measured by recording the absorption peak of MB in the range of 200-800 nm at regular time intervals using the UV-vis spectrophotometer. The reduction in the intensity of the absorption peak of the MB at 665 nm reflects the decrease in the dye concentration in the solution. Therefore, MB degradation was calculated in terms of the percentage of degradation using the following equation (Boruah *et al*., 2021):

$$\% \text{ total removal} = \frac{A_0 - A_t}{A_0} \times 100 \quad (3)$$

where A_0 is the initial absorbance of the dye solution, and A_t is the absorbance of the dye solution after photocatalytic degradation.

3 Results

3.1 Synthesis of AuNPs with different volumes of the extract

Since the HE extract acts as a reducing and stabilizing agent during the synthesis of AuNPs, it is essential to find the correct extract concentration to achieve sufficient reduction and stabilization (Aji *et al*., 2022). Figure 1a depicts the UV-vis absorption spectra of the NPs using $HAuCl_4$ (1mM) and different amounts of the pure extract (0.2, 0.4, 0.6, 0.8, and 1 mL).

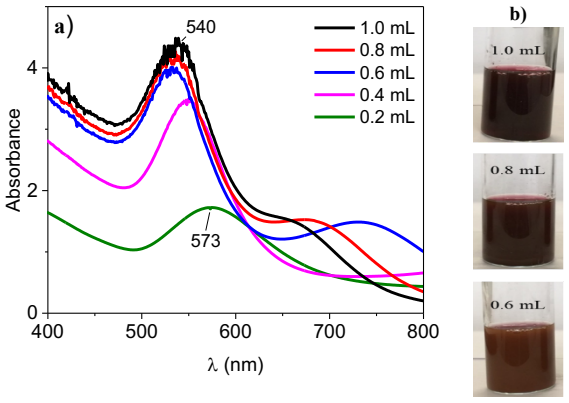

Figure 1. (a) UV-vis spectrum of PHE-AuNPs, (b) optical images of PHE-AuNPs synthesized with different volumes of the HE extract. Reaction time, 120 min.

The samples are denominated PHE-AuNPs. The SPR-associated band is observed between 540 and 573 nm, it clearly indicates the reduction of Au^{3+} to Au^{0} and the formation of spherical AuNPs (Khatua *et al*., 2020; Mariychuk *et al*., 2020; Serrano-Niño *et al*., 2020). The band of NPs synthesized with 0.2 mL of the extract is located at ~573 nm, suggesting aggregated nanoparticles due to insufficient protective coating (Mzwd *et al*., 2022; Vo *et al*., 2022). However, as the volume of the extract increases, an increase in absorbance is observed. Also, a blue shift appears (~540 nm), especially in the samples synthesized with 0.6, 0.8, and 1 mL of extract. The increase in absorbance is related to the increased concentration of NPs (Mzwd *et al*., 2022). The blue shift reveals a decrease in particle size (Chen *et al*., 2019; Mzwd *et al*., 2022). This behavior could be attributed to a higher amount of extract, which reduces gold ions and prevents the agglomeration of NPs (Chen *et al*., 2019; Fan *et al*., 2020). In addition, the samples synthesized with 0.6, 0.8, and 1 mL of the extract demonstrate an additional band at wavelengths >700 nm, related to non-spherical NPs (Mariychuk *et al*., 2020).

The color change during the reaction, from yellow to dark purple, indicates that AuNPs have been formed (Fig. 1b) (Chen *et al*., 2019; Mariychuk *et al*., 2020). The color change in nanoparticles appears to be due to the SPR phenomenon. This phenomenon is due in turn to the excitation of the free electrons in the conduction band, generating the collective oscillation of all of the electrons (Aji *et al*., 2022).

Figure 2 presents the UV-vis spectra of NPs synthesized with the diluted extract and $HAuCl_4$ (1 mM), denominated DHE-AuNPs. As the volume of extract increases, the absorbance increases, and a blue shift is observed. Even the sample synthesized with 1 mL of extract presents a narrower band, suggesting monodispersing sizes. Moreover, when the diluted extract is used, the intensity of the bands at wavelengths >700 nm decreases or disappears,

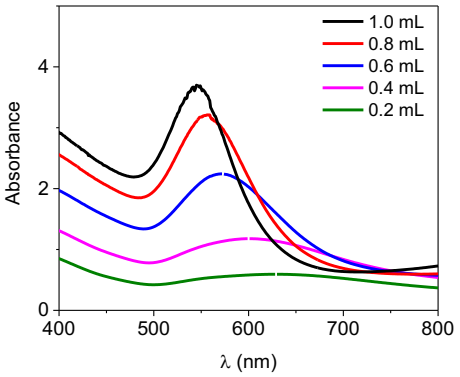

Figure 2. UV-vis spectra of DHE-AuNPs. Reaction time, 120 min.

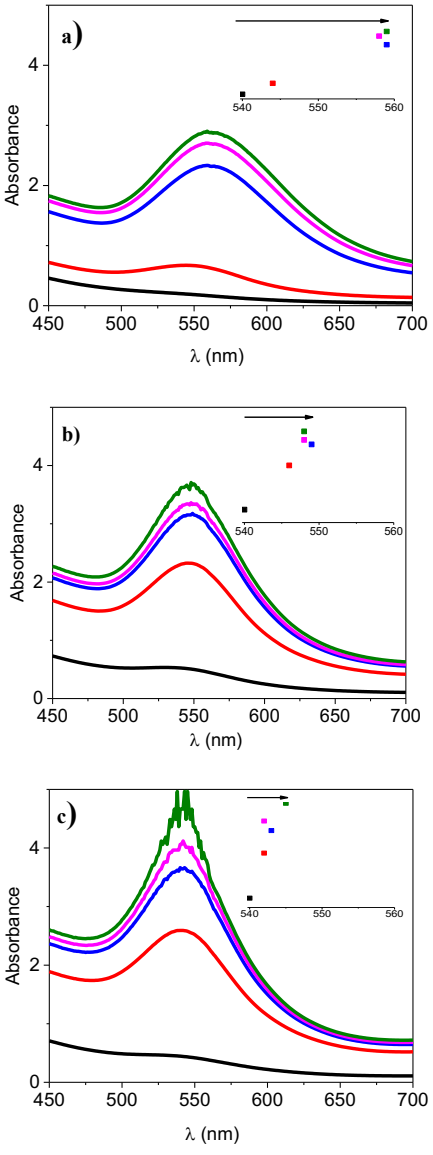

Figure 3. UV-vis spectra of DHE-AuNP synthesized at various times using (a) 0.6, (b) 0.8 and (c) 1 ml of the HE extract.

suggesting that the samples contain mostly spherical NPs (Aji *et al*., 2022).

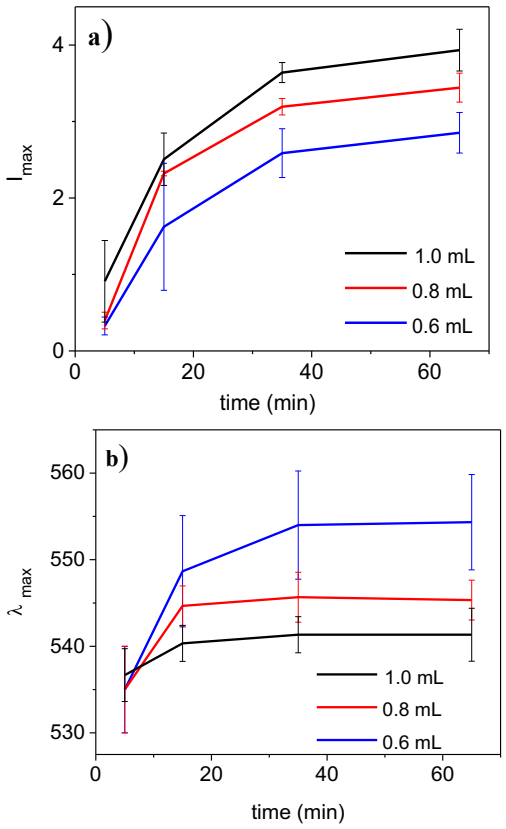

Figure 4. Kinetics of DHE-AuNPs formation: (a) I_{max} vs. time and (b) λ_{max} vs. time. Solid lines are visual aids. Error bars indicate the standard deviations (SD) for the measurements taken in triplicate.

Figure 3 shows the effect of reduction time in the synthesis of DHE-AuNPs. In the three colloidal solutions, a red-shift is observed. The NPs synthesized employing 0.6 mL of extract (Fig. 3a) exhibit broad bands with low absorbance. The NPs synthesized with 0.8 and 1 mL of extract reveal narrower bands with higher absorbance (Fig. 3b and 3c). As the amount of extract increases, a decrease in red-shift is observed (see the λ in the inserts), suggesting that 0.8 and 1 mL of the extract are optimal for the control of particle growth (Du *et al*., 2020).

The green synthesis of metallic NPs is still not completely understood, but there is a proposed mechanism that suggests three stages. (1) bioreduction of metal ions (from Au^{3+} to Au^{0}) due to the presence of reducing molecules, such as antioxidants, in the plant extract. (2) growth phase, Au^{0} forms gold clusters by combining spontaneously. The clusters act as the nucleation center and further promote the reduction of the remaining gold ions. Finally, (3) the termination phase, where the final form of the NPs is defined (Kumari & Meena, 2020; J. Singh *et al*., 2018).

Figure 4 presents the maximal absorbance (I_{max}) and maximal wavelength (λ_{max}) of the SPR bands of the DHE-AuNPs. I_{max} increases with the increasing amount of extract, indicating the formation of a higher amount of AuNPs, especially in the sample synthesized with 1 mL (Fig. 4a) (Aji *et al*., 2022; Mzwd *et al*., 2022). All samples reached equilibrium after 60 minutes, indicating good colloidal stability (Aji *et al*., 2022). The colloidal solution synthesized with 1ml of HE extract also exhibits a lower λ_{max}, suggesting smaller AuNPs (Fig. 4b) (Irfan *et al*., 2016). Therefore, 1 mL of the HE extract was selected as the optimal volume for the synthesis of the NPs. In the next stage, we will work with this sample, denominated D1HE-AuNPs.

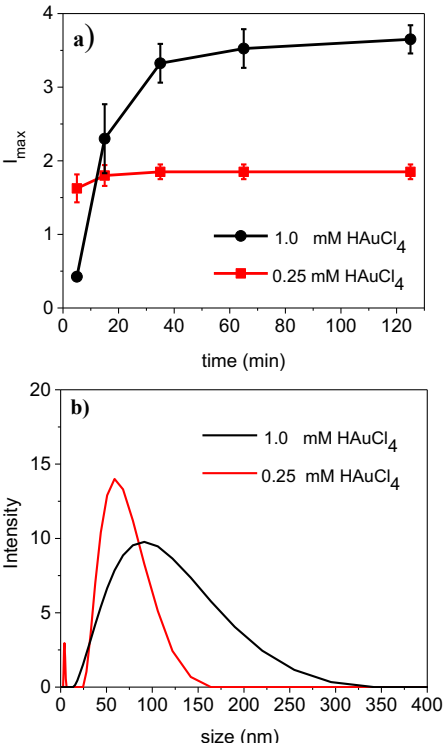

Figure 5. (a) I_{max} vs. time, solid lines are visual aids and error bars that indicate the standard deviations (SD) for measurements in triplicate; (b) Hydrodynamic diameter determined by DLS of D1HE-AuNPs using 0.25 and 1.0 mM of $HAuCl_4$.

3.2 Synthesis of D1HE-AuNPs by modifying the concentration of HAuCL$_4$

Figure 5a presents the I_{max} vs. time of the D1HE-AuNPs samples synthesized with $HAuCl_4$, 0.25, and 1.0 mM. NPs synthesized with $HAuCl_4$ at 1.0 mM exhibit a higher I_{max}, suggesting greater NPs production. This result is expected, in that a larger amount of precursor was used. Seku *et al*. (2019), have demonstrated that, by increasing the concentration of $HAuCl_4$, the amount of AuNPs also increases. On the other hand, NPs size is confirmed by DLS. The DLS technique measures the hydrodynamic diameter. This diameter includes any biomolecules adsorbed onto its surface (Rey-Méndez *et al*., 2022). Figure 5b depicts the particle size distribution of the D1HE-AuNPs

samples synthesized with 0.25 mM (red line) and 1.0 mM (black line) of $HAuCl_4$. The sample prepared with 0.25 mM of $HAuCl_4$ exhibits an abundance ranging from 25-160-nm particles. The average hydrodynamic diameter is 41 nm, and the Z-potential is -28.6 mV. The sample synthesized utilizing 1.0 mM of $HAuCl_4$ reveals sizes of between 15 and 300 nm. The average hydrodynamic diameter is 60 nm, and the Z-potential is -30.9 mV. The high negative value evidenced that the NPs form a stable colloidal solution (Aji *et al*., 2022). The negative surface charge is attributed to the biomolecules adsorbed onto the surface of the AuNPs. These biomolecules form an organic layer around the particles, preventing their agglomeration (Aji *et al*., 2022; Rey-Méndez *et al*., 2022). Different authors suggest that large particle size may be due to NPs with multiple protective layers (Parial & Pal, 2015; Rey-Méndez *et al*., 2022), the large size can be caused by various interaction forces in the solution, including Van der Waals forces (Aji *et al*., 2022; Khlebtsov & Khlebtsov, 2011; Rey-Méndez *et al*., 2022).

TEM images of the sample D1HE-AuNPs using 0.25 mM of $HAuCl_4$ showed spherical particles with an average size of 27.3 ± 5.9 nm (Fig. 6a). Additionally, the TEM results of the sample employing 1 mM $HAuCl_4$ confirm that the particles are spherical and that, based on the histogram, the average particle size is 17.1 ± 6.8 nm (Fig. 6b). Both images reveal gray shadows that could be related to the extract. The size of AuNPs obtained by DLS was larger compared to TEM images. This is because the TEM measurement provides the size of the core of the metallic NPs, and the DLS measures the core and the biomolecules attached to it (Aji *et al*., 2022).

The thickness of the protective organic layers often affects the properties of the AuNPs. The thick organic layers can inhibit the physical contact of the metal surface with the targets (Aji *et al*., 2022). To measure the antioxidant and photocatalytic properties, AuNPs were employed: (1) directly (D1HE-AuNPs), and (2) centrifuged and washed (D1HE-AuNPs W). The size and morphology of the centrifuged and washed NPs were measured by DLS and TEM. In both samples, DLS reveals an increase in size, suggesting agglomeration (Fig. 7a). The sample prepared with 0.25 mM of $HAuCl_4$ exhibits sizes between 60 and 250 nm, while NPs prepared with 1.0 mM of $HAuCl_4$ depict sizes between 35 and 400 nm. In the first case, TEM micrographs demonstrate agglomerated NPs (Fig. 7b). Some branched particles with sizes ranging from 30-60 nm even appear (Fig. 7c). Residual gold ions or tiny NPs probably agglomerated under centrifugation, causing anisotropic growth of the particles (Osonga *et al*., 2022). In the second case, apparently, the particles retained their shape and size. However, under centrifugation, they agglomerated (Fig. 7d and 7e). In both cases, the gray shadow disappears, suggesting partial removal of the HE extract.

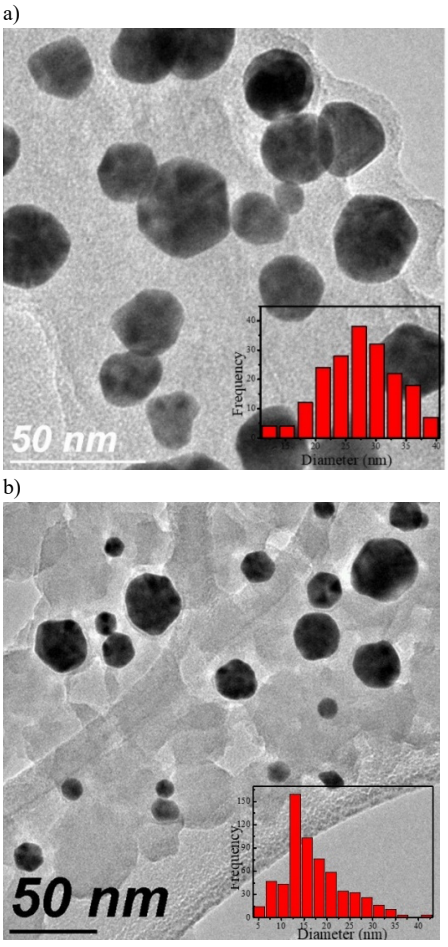

Figure 6. TEM images of the D1HE-AuNPs synthesized with $HAuCl_4$ (a) 0.25 mM, and (b) 1 mM. Inset corresponds to the size-distribution histogram.

The crystalline nature of the D1HE-AuNPs was confirmed by XRD analysis. As shown in Figure 8, the AuNPs shows five diffraction peaks at 2θ = 38.2, 44.5, 64.5, 77.6, and 81.6 related to the (111), (200), (220), (311), and (222) planes of the face-centered cubic (fcc) structure, indicating that the AuNPs are crystalline in nature (JCPDS 04-0783)(Cordero-García *et al*., 2023; Du *et al*., 2020). These findings agree with previous research using *Pogestemon benghalensis* (B) *O. Ktz* or *Parkia roxburghii* leaf extract for AuNP synthesis (Paul *et al*., 2015, 2016). The XRD pattern supports the presence of gold nanomaterials, as seen in UV-Vis spectra and TEM images.

3.3 Antioxidant activity tests

DPPH and ABTS are methods commonly used to investigate the antioxidant potential of plant extracts. The antioxidant activity at different concentrations (ranging from 10 μL/mL-50 μL/mL) of HE extract was examined by DPPH and ABTS scavenging

assay. It was found (Fig. 9) that scavenging activity increases with the increase in the concentration of HE extract due to inhibition of the interaction with free radicals, reaching a percentage of inhibition of 90 % at a concentration of 50 μL/mL. According to Chahardoli *et al*. (2017), the *Nigella arvensis* leaf extract showed an inhibition percentage of only 35% at a concentration of 500 mg/mL. Therefore, the extract obtained in this work exhibited a higher inhibition percentage at a lower concentration, indicating that it has much higher antioxidant activity.

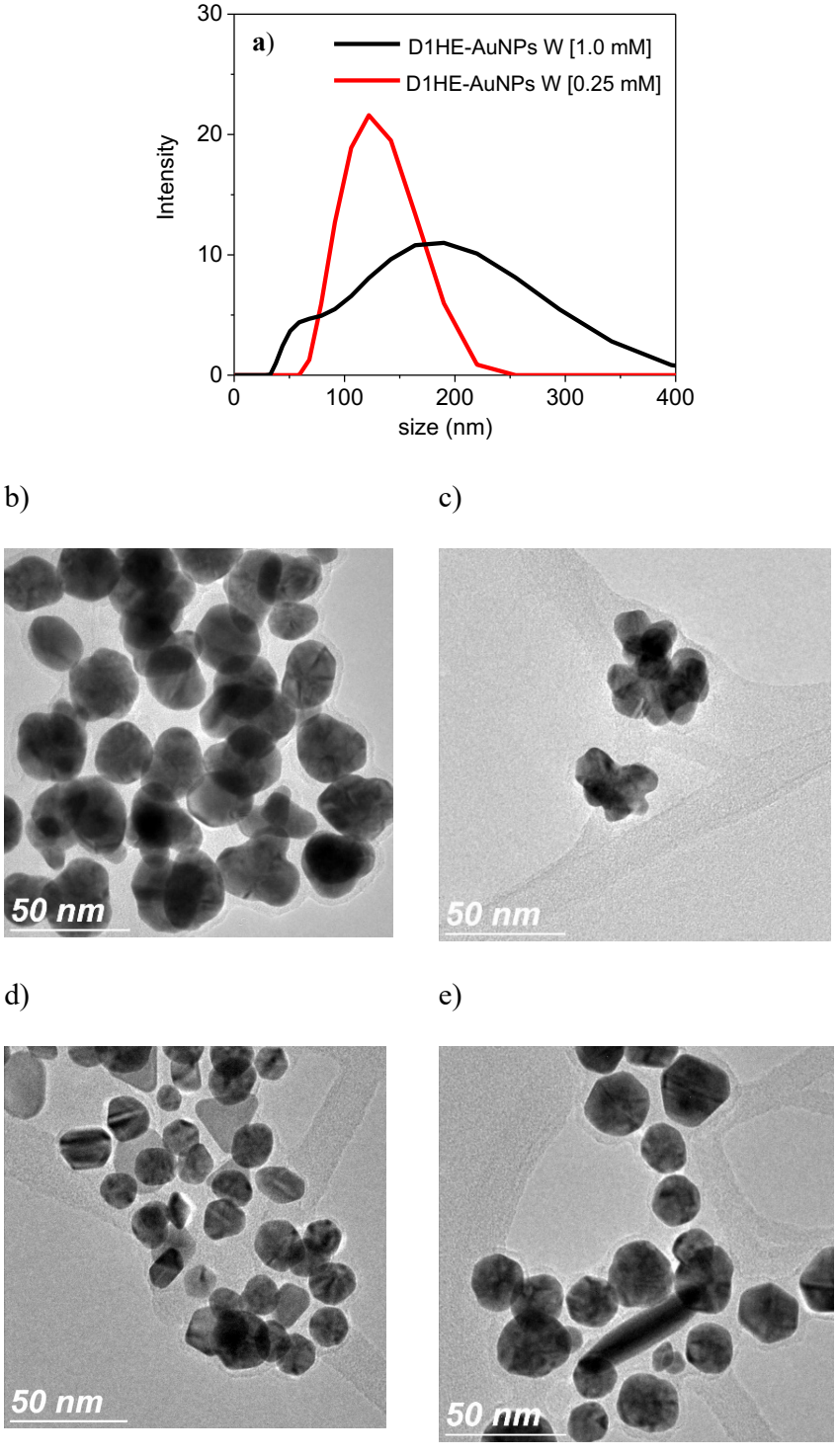

Figure 7. (a) Particle size distribution of D1HE-AuNPs W; (b, c) TEM micrographs for washed particles synthesized with 0.25 mM of $HAuCl_4$; (d, e) TEM micrographs for washed particles synthesized with 1. 0 mM of $HAuCl_4$.

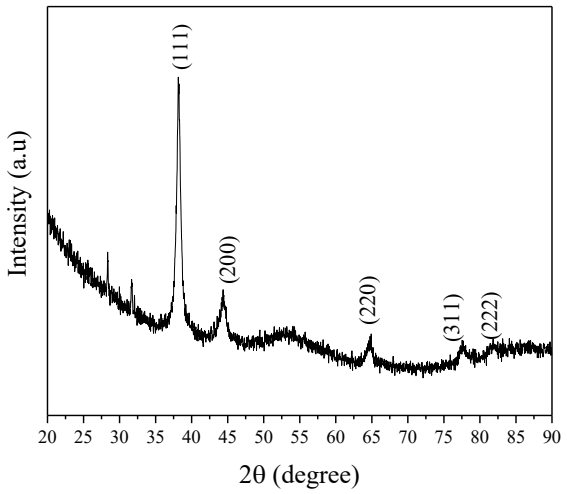

Figure 8. XRD pattern of the D1HE-AuNPs synthesized with $HAuCl_4$ 1 mM.

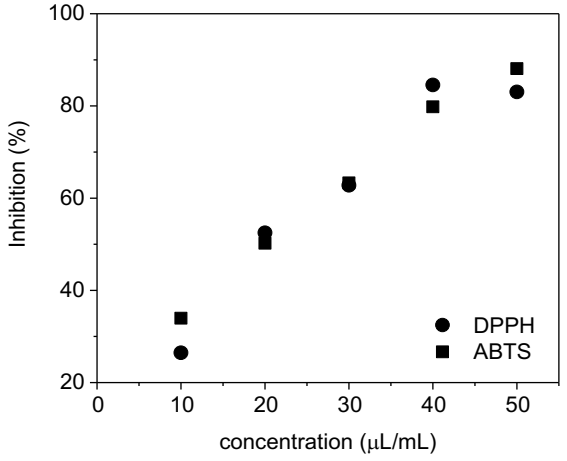

Figure 9. DPPH and ABTS scavenging activity of the HE extract at various concentrations.

The IC_{50} value is a crucial metric in determining the potency of a substance in combating free radicals. It measures the concentration at which the initial concentration of the free radical is halved (Baruah *et al*., 2018). The IC_{50} value of the scavenging-activity value of the HE extract is 20 μL/mL for both the DPPH and the ABTS methods. The IC_{50} values of licorice root (*Glycyrrhzia glabra* L.) extract by DPPH and ABTS methods were 86.90 and 83.81 mg/mL, respectively (Al-Radadi, 2021). The lower IC_{50} value indicates higher antioxidant activity; therefore, the HE extract has higher antioxidant activity than the licorice extract.

Among the compounds found in the extract are canophyllol, pristimerin, celastrol, and galactitol (Reyes-Chilpa *et al*., 2003). However, according to Munteanu & Apetrei (2021), several factors affect the efficacy of antioxidant compounds, the most important of which are structural properties, temperature, concentration, characteristics of the substrate susceptible to oxidation, along with the presence of synergistic and pro-oxidant compounds and the physical state of the system.

Table 1. Percentages of inhibition obtained for the AuNPs.

Samples	ABTS	DPPH
D1HE-AuNPs [$HAuCl_4$ 0.25 mM]	**37.5**	**82.1**
D1HE-AuNPs W [$HAuCl_4$ 0.25 mM]	5.46	9.7
D1HE-AuNPs [$HAuCl_4$ 1 mM]	**14.5**	**28.2**
D1HE-AuNPs W [$HAuCl_4$ 1 Mm]	3.8	5.8

For the unwashed (D1HE-AuNPs) and washed (D1HE-AuNPs W) nanoparticles, their antioxidant activity was measured directly without dilution; the percentages of inhibition obtained are presented in Table 1. The percentages of inhibition were higher for the D1HE-AuNPs. NPs synthesized with $HAuCl_4$ [0.25 mM] are highlighted for their efficiency, presenting the highest percentage of inhibition in the scavenging of ABTS and DPPH radicals. Zayed *et al*. (2020), note that the antioxidant activity is attributed to the phenolic compounds in the extract that coat the NPs and that are found in the medium. It is suggested that the unwashed AuNPs possess a higher coating of phenolic compounds from the HE extract; consequently, they achieve higher percentages of inhibition.

Overall, the antioxidant activity of the HE extract was much higher than the antioxidant activity of AuNPs. Our results are in agreement with those of the study of Nakkala *et al*. (2015, 2016), whose authors reported that the antioxidant activity of the *Costus pictus* and *Piper longum* plant extracts was higher than that of biosynthesized AuNPs. Likewise, Kuppusamy *et al*. (2015), obtained similar results using green-synthesized AuNPs from *Commelina nudiflora*. Phenolic compounds from HE extract may have coated the nanoparticles, leading to their DPPH scavenging activity. In addition, the electronic configurations of AuNPs can accept or donate an electron to scavenge the free radical (Zayed *et al*., 2020). Food scientists and medical professionals are interested in natural antioxidants because they protect food from spoilage and the body from oxidative stress.

3.4 Photocatalytic activity tests

This study aimed to evaluate the catalytic properties of AuNPs for the reduction and degradation of MB dye as a model reaction. The MB was degraded at different times in the presence of D1HE-AuNPs

utilizing $HAuCl_4$ 0.25 mM (unwashed and washed). The spectra analysis revealed that pure MB (0 min) exhibits a main absorption peak at 664 nm, which corresponds to n-π^* transition, and a shoulder peak at 614 nm (Kumar *et al*., 2016). Figure 10a shows the UV-vis spectra of MB degradation employing the unwashed AuNPs. The colloidal solution reveals a high percentage of adsorption of MB (about 70%), possibly due to the extract adsorbed onto the AuNPs. According to Paul *et al*. (2015), the extract has been found to prevent the agglomeration of NPs, resulting in better dye adsorption and improved photocatalytic activity. The data clearly shows a gradual decrease in absorbance, which resulted in a significant reduction of MB (90 min). It is evident that the colloidal AuNPs played a crucial role in this process by acting as an electron transfer mediator. The unreacted phytochemicals of the HE extract undergo a redox reaction with MB due to the electron relay effect facilitated by the AuNPs. This finding is consistent with the research conducted by Kumar *et al*. (2016). The total percentage of dye removal was 89%. The degradation of MB in the absence of NPs was investigated, the response of which was only 19%.

On the other hand, MB degradation was monitored using washed AuNPs (Fig. 10b). The washing process removes the extract and, as the TEM images show, some NPs agglomerate or fuse, giving rise to an increase in particle size. The adsorption percentage of MB decreases to 35%, achieving a total removal of 70%.

Figure 10c shows the plot of $-\ln(C/C_0)$ vs. time for the photocatalytic degradation of MB solutions using both samples. The rate constant derived from Figure 10c amounts to 0.02847 and 0.01568 min^{-1} for the unwashed and washed NPs, respectively. The regression coefficient values for these samples were 0.945 and 0.941, respectively, which indicates that the experimental data are fit to a pseudo first-order kinetic model (Baruah *et al*., 2018; Kumar *et al*., 2016).

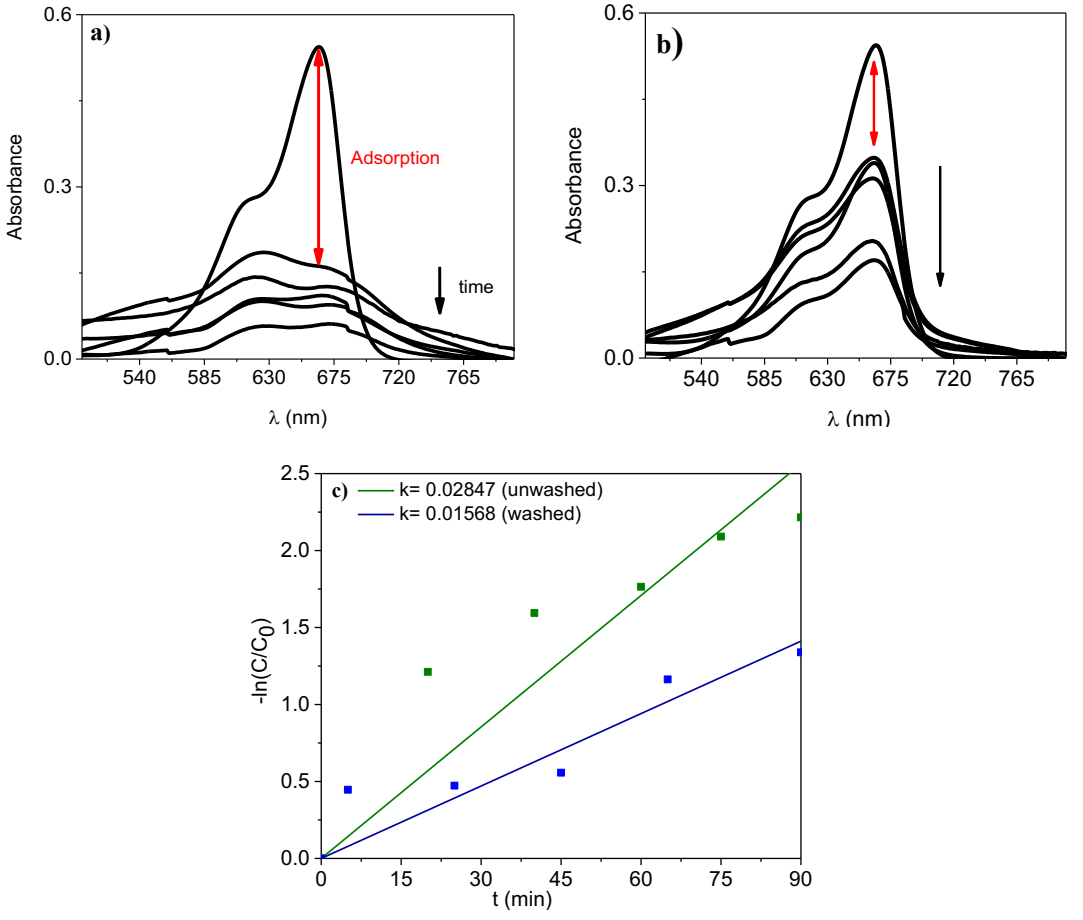

Figure 10. UV-vis spectrum of MB degradation using (a) unwashed, (b) washed AuNPs, and (c) plot of $-\ln(C/C_0)$ vs. time.

Conclusions

In the present study, gold nanoparticles were synthesized using the extract of the root bark of *Hippocratea excelsa*, an endemic plant of Mexico with medicinal properties. UV-vis spectroscopy confirmed the successful biosynthesis of AuNPs and increasing the extract volume resulted in a higher number of NPs. Furthermore, the size distribution of the NPs obtained through DLS indicates that they have a protective layer, making them stable and resistant to aggregation. TEM images demonstrate that the AuNPs are mostly spherical with sizes of 27 nm, and the XRD pattern confirms the presence of gold nanomaterials. The findings also reveal that the extract has potent antioxidant properties, and so do the AuNPs. The AuNPs synthesized with 0.25 mM of $HAuCl_4$ unwashed revealed the highest percentage of inhibition of antioxidant activity. Additionally, this sample shows a high percentage of MB adsorption, which resulted in a total percentage of dye removal of 89%. These results show that the AuNPs produced by ecological, simple, and cost-effective methods are viable candidates for different applications.

Acknowledgment

The authors are very grateful to Francisco Ruiz and Jaime Mendoza for their technical support with TEM measurements at CNyN-UNAM. This research was financially supported by the Benemérita Universidad Autónoma de Puebla VIEP 2022, 2023.

References

Aguilar-Pliego, J., Nuñez, R. Z., Agundez, J., De la Serna Valdés, R. and Pérez-Pariente, J. (2021). Biosynthesis of gold clusters and nanoparticles by using extracts of Mexican plants and evaluation of their catalytic activity in oxidation reactions. *Catalysis Letters 151*, 1604-1611. https://doi.org/10.1007/s10562-020-03416-4

Aji, A., Oktafiani, D., Yuniarto, A. and Amin, A. K. (2022). Biosynthesis of gold nanoparticles using Kapok (*Ceiba pentandra*) leaf aqueous extract and investigating their antioxidant activity. *Journal of Molecular Structure 1270*, 133906. https://doi.org/10.1016/j.molstruc.2022.133906

Alanís, A. D., Calzada, F., Cervantes, J. A., Torres, J. and Ceballos, G. M. (2005). Antibacterial properties of some plants used in Mexican traditional medicine for the treatment of gastrointestinal disorders. *Journal of Ethnopharmacology 100*, 153-157. https://doi.org/10.1016/j.jep.2005.02.022

Al-Radadi, N. S. (2021). Facile one-step green synthesis of gold nanoparticles (AuNp) using licorice root extract: Antimicrobial and anticancer study against HepG2 cell line. *Arabian Journal of Chemistry 14*, 102956. https://doi.org/10.1016/j.arabjc.2020.102956

Apaza Ticona, L., Slowing, K., Serban, A. M., Humanes Bastante, M. and Hernáiz, M. J. (2022). Wound healing, anti-inflammatory and anti-melanogenic activities of ursane-type triterpenes from *Semialarium mexicanum* (Miers) Mennega. *Journal of Ethnopharmacology 289*, 115009. https://doi.org/10.1016/j.jep.2022.115009

Baruah, D., Goswami, M., Yadav, R. N. S., Yadav, A. and Das, A. M. (2018). Biogenic synthesis of gold nanoparticles and their application in photocatalytic degradation of toxic dyes. *Journal of Photochemistry and Photobiology B: Biology 186*, 51-58. https://doi.org/10.1016/j.jphotobiol.2018.07.002

Boruah, J. S., Devi, C., Hazarika, U., Bhaskar Reddy, P. V., Chowdhury, D., Barthakur, M. and Kalita, P. (2021). Green synthesis of gold nanoparticles using an antiepileptic plant extract:in vitrobiological and photo-catalytic activities. *RSC Advances 11*, 28029-28041. https://doi.org/10.1039/d1ra02669k

Cáceres-Castillo, D., Mena-Rejón, G. J., Cedillo-Rivera, R. and Quijano, L. (2008). 21β-Hydroxy-oleanane-type triterpenes from *Hippocratea excelsa*. *Phytochemistry 69*, 1057-1064. https://doi.org/10.1016/j.phytochem.2007.10.016

Calzada, F. and Mata, R. (1995). Hippocrateine III, a sesquiterpene alkaloid from *Hippocratea excelsa*. *Phytochemistry 40*, 583-585. https://doi.org/10.1016/0031-9422(95)00255-6

Chahardoli, A., Karimi, N., Sadeghi, F. and Fattahi, A. (2018). Green approach for synthesis of gold nanoparticles from *Nigella arvensis* leaf extract and evaluation of their antibacterial, antioxidant, cytotoxicity and catalytic activities. *Artificial Cells, Nanomedicine and Biotechnology 46*, 579-588. https://doi.org/10.1080/21691401.2017.1332634

Chen, M. N., Chan, C. F., Huang, S. L. and Lin, Y. S. (2019). Green biosynthesis of gold nanoparticles using *Chenopodium formosanum* shell extract and analysis of the particles' antibacterial properties. *Journal of the Science of Food and Agriculture 99*, 3693-3702. https://doi.org/10.1002/jsfa.9600

Conde-Hernández, L. A. and Guerrero-Beltrán, J. Á. (2014). Total phenolics and antioxidant activity of *Piper auritum* and *Porophyllum ruderale*. *Food Chemistry 142*, 455-460. https://doi.org/10.1016/j.foodchem.2013.07.078

Cordero-García, M. X., Rojas-García, E., Salinas-Rodríguez, E. and Gómez, S. A. (2023). Influence on pretreatment in CeO_2 and Au/CeO_2 nanocomposite to improve the creation of surface defects enabling modification in optical interband. *Revista Mexicana de Ingeniería Química 22*, Mat2991. https://doi.org/10.24275/rmiq/Mat2991

Doan, V. D., Thieu, A. T., Nguyen, T. D., Nguyen, V. C., Cao, X. T., Nguyen, T. L. H. and Le, V. T. (2020). Biosynthesis of gold nanoparticles using *Litsea cubeba* fruit extract for catalytic reduction of 4-Nitrophenol. *Journal of Nanomaterials 2020*, 4548790. https://doi.org/10.1155/2020/4548790

Du, J., Wu, S., Hu, Z., Yu, Z., Zhao, D. and Bai, Y. (2020). Green synthesis of salt-tolerant gold nanoparticles for the rapid qualitative detection of *Listeria monocytogenes* in lateral flow immunoassay. *Journal of Materials Science 55*, 15426-15438. https://doi.org/10.1007/s10853-020-05118-z

El-Borady, O. M., Ayat, M. S., Shabrawy, M. A. and Millet, P. (2020). Green synthesis of gold nanoparticles using Parsley leaves extract and their applications as an alternative catalytic, antioxidant, anticancer, and antibacterial agents. *Advanced Powder Technology 31*, 4390-4400. https://doi.org/10.1016/j.apt.2020.09.017

Escobedo Hinojosa, W. I., Acevedo Quiróz, M., Romero Álvarez, I., Escobar Castañeda, P., Villarreal, M. L. and Taketa, A. C. (2014). Anti-Helicobacter pylori, gastroprotective, anti-inflammatory, and cytotoxic activities of methanolic extracts of five different populations of *Hippocratea celastroides* collected in Mexico. *Journal of Ethnopharmacology 155*, 1156-1163. https://doi.org/10.1016/j.jep.2014.06.044

Fan, J., Cheng, Y. and Sun, M. (2020). Functionalized gold nanoparticles: synthesis, properties and biomedical applications. *The Chemical Record 20*, 1474-1504. https://doi.org/10.1002/tcr.202000087

Furukawa, M., Furukawa, M., Makino, M., Uchiyama, T., Fujimoto, Y. and Matsuzaki, K. (2018). New sesquiterpene pyridine alkaloids from *Hippocratea excelsa*. *Natural Product Communications 13*, 957-960. https://doi.org/10.1177/1934578x1801300809

Furukawa, M., Makino, M., Uchiyama, T., Ishimi, K., Ichinohe, Y. and Fujimoto, Y. (2002). Sesquiterpene pyridine alkaloids from *Hippocratea excelsa*. *Phytochemistry 59*, 767-777. https://doi.org/https://doi.org/10.1016/S0031-9422(02)00020-1

Irfan, M., Ahmad, T., Moniruzzaman, M. M., Abdullah, B. B. and Bhattacharjee, S. (2016). Ionic liquid mediated biosynthesis of gold nanoparticles using *Elaeis guineensis* (oil palm) leaves extract. *Procedia Engineering 148*, 568-572. https://doi.org/10.1016/j.proeng.2016.06.512

Kamran, U., Bhatti, H. N., Iqbal, M. and Nazir, A. (2019). Green synthesis of metal nanoparticles and their applications in different fields: A review. *Zeitschrift fur Physikalische Chemie 233*, 1325-1349. https://doi.org/10.1515/zpch-2018-1238

Keijok, W. J., Pereira, R. H. A., Alvarez, L. A. C., Prado, A. R., da Silva, A. R., Ribeiro, J., de Oliveira, J. P. and Guimarães, M. C. C. (2019). Controlled biosynthesis of gold nanoparticles with *Coffea arabica* using factorial design. *Scientific Reports 9*, 16019. https://doi.org/10.1038/s41598-019-52496-9

Khatua, A., Prasad, A., Priyadarshini, E., Patel, A. K., Naik, A., Saravanan, M., Barabadi, H., Ghosh, llora, Paul, B., Paulraj, R. and Meena, R. (2020). Emerging antineoplastic plant-based gold nanoparticle synthesis: a mechanistic exploration of their anticancer activity toward cervical cancer cells. *Journal of Cluster Science 31*, 1329-1340. https://doi.org/10.1007/s10876-019-01742-1

Khlebtsov, B. N. and Khlebtsov, N. G. (2011). On the measurement of gold nanoparticle sizes by the dynamic light scattering method. *Colloid Journal 73*, 118-127. https://doi.org/10.1134/S1061933X11010078

Kumar, B., Smita, K., Cumbal, L. and Debut, A. (2016). One pot synthesis and characterization

of gold nanocatalyst using Sacha inchi (*Plukenetia volubilis*) oil: Green approach. *Journal of Photochemistry and Photobiology B: Biology 158*, 55-60. https://doi.org/10.1016/j.jphotobiol.2016.02.023

Kumari, P. and Meena, A. (2020). Green synthesis of gold nanoparticles from *Lawsoniainermis* and its catalytic activities following the Langmuir-Hinshelwood mechanism. *Colloids and Surfaces A: Physicochemical and Engineering Aspects 606*, 125447. https://doi.org/10.1016/j.colsurfa.2020.125447

Kuppusamy, P., Yusoff, M. M., Parine, N. R. and Govindan, N. (2015). Evaluation of in-vitro antioxidant and antibacterial properties of *Commelina nudiflora* L. extracts prepared by different polar solvents. *Saudi Journal of Biological Sciences 22*, 293-301. https://doi.org/10.1016/j.sjbs.2014.09.016

Kurhade, P., Kodape, S. and Choudhury, R. (2021). Overview on green synthesis of metallic nanoparticles. *Chemical Papers 75*, 5187-5222. https://doi.org/10.1007/s11696-021-01693-w

Mariychuk, R., Grulova, D., Grishchenko, L. M., Linnik, R. P. and Lisnyak, V. V. (2020). Green synthesis of non-spherical gold nanoparticles using *Solidago canadensis* L. extract. *Applied Nanoscience 10*, 4817-4826. https://doi.org/10.1007/s13204-020-01406-x

Mata, R., Calzada, F., Díaz, E. and Toscano, R. A. (1990). Chemical studies on Mexican plants used in traditional medicine, XV. Sesquiterpene evoninoate alkaloids from *Hippocratea excelsa*. *Journal of Natural Products 53*, 1212-1219. https://doi.org/10.1021/np50071a012

Mena-Rejón, G. J., Pérez-Espadas, A. R., Moo-Puc, R. E., Cedillo-Rivera, R., Bazzocchi, I. L., Jiménez-Diaz, I. A. and Quijano, L. (2007). Antigiardial activity of triterpenoids from root bark of *Hippocratea excelsa*. *Journal of Natural Products 70*, 863-865. https://doi.org/10.1021/np060559y

Munteanu, I. G. and Apetrei, C. (2021). Analytical methods used in determining antioxidant activity: A review. *International Journal of Molecular Sciences 22*, 3380. https://doi.org/10.3390/ijms22073380

Mzwd, E., Ahmed, N. M., Suradi, N., Alsaee, S. K., Altowyan, A. S., Almessiere, M. A. and Omar, A. F. (2022). Green synthesis of gold nanoparticles in Gum Arabic using pulsed laser ablation for CT imaging. *Scientific Reports 12*, 10549. https://doi.org/10.1038/s41598-022-14339-y

Nakkala, J. R., Bhagat, E., Suchiang, K. and Sadras, S. R. (2015). Comparative study of antioxidant and catalytic activity of silver and gold nanoparticles synthesized from *Costus pictus* leaf extract. *Journal of Materials Science and Technology 31*, 986-994. https://doi.org/10.1016/j.jmst.2015.07.002

Nakkala, J. R., Mata, R. and Sadras, S. R. (2016). The antioxidant and catalytic activities of green synthesized gold nanoparticles from *Piper longum* fruit extract. *Process Safety and Environmental Protection 100*, 288-294. https://doi.org/10.1016/j.psep.2016.02.007

Navarrete, A., Luis Trejo-Miranda, J. and Reyes-Trejo, L. (2002). Principles of root bark of *Hippocratea excelsa* (Hippocrataceae) with gastroprotective activity. *Journal of Ethnopharmacology 79*, 383-388. https://doi.org/10.1016/S0378-8741(01)00414-7

Osonga, F. J., Eshun, G. B. and Sadik, O. A. (2022). Ligand effect on controlling the synthesis of branched gold nanomaterials against fusarium wilt diseases. *RSC Advances 12*, 31855-31868. https://doi.org/10.1039/d2ra05478g

Parial, D., & Pal, R. (2015). Biosynthesis of monodisperse gold nanoparticles by green alga *Rhizoclonium* and associated biochemical changes. *Journal of Applied Phycology 27*, 975-984. https://doi.org/10.1007/s10811-014-0355-x

Paul, B., Bhuyan, B., Dhar Purkayastha, D., Dey, M. and Dhar, S. S. (2015). Green synthesis of gold nanoparticles using *Pogestemon benghalensis* (B) O. Ktz. leaf extract and studies of their photocatalytic activity in degradation of methylene blue. *Materials Letters 148*, 37-40. https://doi.org/10.1016/j.matlet.2015.02.054

Paul, B., Bhuyan, B., Purkayastha, D. D. and Dhar, S. S. (2016). Photocatalytic and antibacterial activities of gold and silver nanoparticles synthesized using biomass of *Parkia roxburghii* leaf. *Journal of Photochemistry and Photobiology B: Biology 154*, 1-7. https://doi.org/10.1016/j.jphotobiol.2015.11.004

Perez, R. M., Perez, S., Zavala, M. A. and Salazar, M. (1995). Anti-inflammatory activity

of the bark of *Hippocratea excelsa*. *Journal of Ethnopharmacology 47*, 85-90. https://doi.org/10.1016/0378-8741(95)01257-E

Reyes-Chilpa, R., Jiménez-Estrada, M., Cristóbal-Telésforo, E., Torres-Colín, L., Villavicencio, M. A., Pérez-Escandón, B. E. and Mercado-González, R. (2003). Natural Insecticides from *Hippocratea excelsa* and *Hippocratea celastroides*. *Economic Botany 57*, 54-64. http://www.jstor.org/stable/4256642

Rey-Méndez, R., Rodríguez-Argüelles, M. C. and González-Ballesteros, N. (2022). Flower, stem, and leaf extracts from *Hypericum perforatum* L. to synthesize gold nanoparticles: Effectiveness and antioxidant activity. *Surfaces and Interfaces 32*, 102181. https://doi.org/10.1016/j.surfin.2022.102181

Seku, K., Gangapuram, B. R., Pejjai, B., Hussain, M., Hussaini, S. S., Golla, N. and Kadimpati, K. K. (2019). Eco-friendly synthesis of gold nanoparticles using carboxymethylated gum *Cochlospermum Gossypium* (CMGK) and their catalytic and antibacterial applications. *Chemical Papers 73*, 1695-1704. https://doi.org/10.1007/s11696-019-00722-z

Serrano-Niño, J. C., Contreras-Martínez, C. A., Pacheco, J. R. S., Ojeda, A. Z., Uscanga, B. R. A. and Cavazos-Garduño, A. (2020). Optimization of the biosynthesis of gold nanoparticles using *Hypericum perforatum* and evaluation of their antimicrobial activity. *Revista Mexicana de Ingeniería Química 19*, 889-902. https://doi.org/10.24275/rmiq/Bio790

Singh, J., Dutta, T., Kim, K. H., Rawat, M., Samddar, P. and Kumar, P. (2018). "Green" synthesis of metals and their oxide nanoparticles: Applications for environmental remediation. *Journal of Nanobiotechnology 16*, 84. https://doi.org/10.1186/s12951-018-0408-4

Singh, T., Jayaprakash, A., Alsuwaidi, M. and Madhavan, A. A. (2020). Green synthesized gold nanoparticles with enhanced photocatalytic activity. *Materials Today: Proceedings 42*, 1166-1169. https://doi.org/10.1016/j.matpr.2020.12.531

Velázquez, C., Calzada, F., Torres, J., González, F. and Ceballos, G. (2006). Antisecretory activity of plants used to treat gastrointestinal disorders in Mexico. *Journal of Ethnopharmacology 103*, 66-70. https://doi.org/10.1016/j.jep.2005.06.046

Vo, Q. K., Nguyen, A. T., Ho, H. T., Huynh, L. T. N., Nguyen, T. P. P. and Nguyen, T. H. T. (2022). Environmentally friendly controlled synthesis of gold nanostars with collagen by one-step reduction method. *Journal of Nanomaterials 2022*, 4046389. https://doi.org/10.1155/2022/4046389

Ying, J., Zheng, Y., Zhang, H. and Fu, L. (2020). Room temperature biosynthesis of gold nanoparticles with *Lycoris aurea* leaf extract for the electrochemical determination of aspirin. *Revista Mexicana de Ingeniería Química 19*, 585-592. https://doi.org/10.24275/rmiq/Mat741

Zayed, M. F., Mahfoze, R. A., El-kousy, S. M. and Al-Ashkar, E. A. (2020). *In vitro* antioxidant and antimicrobial activities of metal nanoparticles biosynthesized using optimized *Pimpinella anisum* extract. *Colloids and Surfaces A: Physicochemical and Engineering Aspects 585*, 124167. https://doi.org/10.1016/j.colsurfa.2019.124167